Pakistan Veterinary Journal

ISSN: 0253-8318 (PRINT), 2074-7764 (ONLINE)
DOI: 10.29261/pakvetj/2026.149

RESEARCH ARTICLE

Evaluation of Traditional Chinese Medicine-Derived Carbon Dots as Antitumor Agents against Canine Mammary Cancer: A Comparative Study with Traditional Decoctions

Qi Chen[1, 2], Biao Liu[1], Zixiang Lin[1], Xinqiu Li[1], Fangying Zhao[1], Chengyu Liu[3], Hong Zhang[3], Wanbing Pan[1, 2], Jiatong Zhang[1, 2], Delanyo Kpeglo[4], Ramadan Taha[5], Maha Abdullah Momenah[6], Etibar Mammadov[7], Wen Chen[3*] and Jiahao Lin[1, 2*]

[1]The Clinical Department, College of Veterinary Medicine, China Agricultural University, Beijing, China; [2]Center of Research and Innovation of Chinese Traditional Veterinary Medicine, China Agricultural University, Beijing, China; [3]Department of Pathology, The 8th Medical Center, Chinese PLA General Hospital, Beijing, China; [4]Leeds Institute of Cardiovascular and Metabolic Medicine, School of Medicine, University of Leeds, Leeds, U.K; [5]Biology Department, Faculty of Science, King Khalid University, P.O. Box 9004, Abha 61413, Saudi Arabia; [6]Department of Biology, College of Science, Princess Nourah bint Abdulrahman University, P.O. Box 84428, Riyadh 11671, Saudi Arabia; [7]Nakhchivan State University, Faculty of Natural Sciences and Agriculture, Veterinary Medicine Department, AZ, 7012, Nakhchivan, Azerbaijan
*Corresponding author: jiahao_lin@cau.edu.cn (Jiahao Lin), chenwen@301hospital.com.cn (Wen Chen).

ARTICLE HISTORY (26-448)

Received: April 23, 2026
Revised: May 24, 2026
Accepted: May 26, 2026
Published online: June 05, 2026

Key words:
Canine mammary tumor
Carbon dots
Traditional Chinese medicine
Traditional decoctions

ABSTRACT

Traditional Chinese medicine (TCM) is widely studied for antitumor drug development, but its decoctions (DECs) are limited by poor solubility and low bioavailability. Although TCM-derived carbon dots (CDs) show promising potential for tumor therapy, no studies have systematically compared whether CDs exhibit superior antitumor efficacy to DECs. In this study, four TCM-derived CDs were systematically compared with their corresponding DECs for antitumor activity both in vitro and in vivo. The results showed that the CDs effectively inhibited the proliferation and migration of CMT-U27 canine mammary tumor cells in vitro, and their inhibitory effect was generally better than those of the corresponding DECs. In vivo mouse assays further indicated that all four CDs effectively inhibited tumor growth with favourable safety profile. However, their antitumor effect was not significantly different from that of the DECs in vivo, which may be due to their small size, leading to rapid clearance from the bloodstream. Therefore, simple bare CDs synthesis may be insufficient to improve the efficacy of TCM against canine mammary cancer, and additional functionalization is required.

To Cite This Article: Chen Q, Liu B, Lin Z, Li X, Zhao F, Liu C, Zhang H, Pan W, Zhang J, Kpeglo D, Taha R, Momenah MA, Mammadov E, Chen W, Lin J, 2026. Evaluation of traditional chinese medicine-derived carbon dots as antitumor agents against canine mammary cancer: a comparative study with traditional decoctions. Pak Vet J, 46(6): 1573-1585. http://dx.doi.org/10.29261/pakvetj/2026.149

INTRODUCTION

Canine mammary tumor, with a malignancy of up to 80%, is the most prevalent spontaneous tumor in female dogs and remains a serious threat to dogs live (Ferreira *et al.,* 2026; Vu *et al.,* 2026). At present, although surgical resection remains the main clinical treatment for canine mammary tumor, drug therapy can effectively reduce the metastasis and recurrence rates of the tumor, and is recognized as a crucial adjunctive therapy for mammary tumor (Beaudu-Lange and Lange, 2024). Modern studies have shown that many traditional Chinese medicines (TCM), such as Hedyotis diffusa (Ma *et al.,* 2019), Scutellaria barbata D.Don (Liu *et al.,* 2022), Forsythia suspensa (Huang *et al.,* 2020) and Agrimonia Pilosa (Yu and Gai, 2023), can inhibit tumor cell proliferation by regulating tumor-related signaling pathways, inducing apoptosis and autophagy, and causing cell cycle arrest, indicating promising potential in tumor therapy. However, TCM mainly relies on traditional processing methods, such as decocting raw medicinal materials with water to prepare decoctions (DECs) (Wu *et al.,* 2025). These methods have several limitations, including poor water solubility, inadequate biodistribution, low bioavailability, and inconsistent quality, which hinder the full utilization of their medicinal value and restrict the modernization of TCM (Tian *et al.,* 2025; Yu *et al.,* 2026). Therefore, the

development and application of novel technologies are essential to overcome its inherent limitations.

The study found that the efficacy of TCM is not entirely attributed to the chemical composition of the drug. The physical state is also an important factor affecting its effect (Yan *et al.,* 2019). When TCM size is reduced to the nanoscale, it can more easily pass through the biofilm by diffusion or osmosis and exert better efficacy (Xie *et al.,* 2025). Carbon dots (CDs) are nanoscale materials with particle size typically below 10 nm, which have good water solubility and biocompatibility (Cohen *et al.,* 2020; Seo *et al.,* 2026). TCM, as a natural product, has gradually become one of the ideal precursors for the synthesis of green CDs (Luo *et al.,* 2021). The ancient Chinese book "Leigong Paozhi Lun", notes that the gap around the container holding TCM was sealed with mud to create a high-temperature, anoxic environment for preparing charcoal medicine, which is similar to one of the synthesis methods of CDs (high-temperature pyrolysis). Furthermore, traditional medical texts such as Xin Xiu Ben Cao and Xiaoer Weisheng Zongwei Lun Fang document the use of charcoal medicines in the treatment of tumors. Modern studies have reported that CDs derived from ginger could significantly inhibit the proliferation of human hepatocellular carcinoma HepG2 cells while exhibiting minimal toxicity towards non-cancerous MCF-10A mammary epithelial cells and FL83B mouse hepatocytes (Li *et al.,* 2014). In addition, Yao et al. found that ginsenoside Re-based CDs could reduce tumor cell proliferation while inducing apoptotic cell death via a caspase-3-mediated pathway (Yao *et al.,* 2018). Therefore, preparing CDs from TCM is expected to be a promising strategy to enhance its antitumor activity.

Because the preparation of CDs involves high pressure and high temperature processing conditions (Fang *et al.,* 2024), the original physicochemical properties and active ingredients of TCM may change during preparation, leading to uncertainty about the pharmacodynamics of TCM CDs. However, there is a lack of comparative studies on the antitumor activity of TCM CDs and traditional DECs. It remains to be seen whether the antitumor effect of CDs made from TCM is enhanced. In this study, CDs synthesized from four representative heat-clearing and detoxifying antitumor TCM were used as the research subject to investigate their antitumor effect in vitro and in vivo, and were compared with the corresponding DECs to evaluate whether CDs preparation enhances their antitumor activity.

MATERIALS AND METHODS

Reagents and materials: Hedyotis diffusa (HD), Scutellaria barbata D.Don (SB), Forsythia suspensa (FS) and Agrimonia Pilosa (AP) were purchased from Beijing Tongrentang. Dulbecco's Modified Eagle's Medium (DMEM), fetal bovine serum (FBS) and penicillin-streptomycin were purchased from Gibco. The CCK-8 kit was purchased from Mei5 Biotechnology Co., Ltd. Capecitabine (CAP) was obtained from Macklin.

Preparation of CDs and DECs: CDs were prepared by hydrothermal treatment. Briefly, 1.6 g of powdered herbs (60 mesh) were dispersed in 240 mL of ultrapure water and heated at 160°C for 8 h in a 300 mL hydrothermal autoclave reactor. After cooling, the supernatant was collected by centrifugation (12,000×g, 30 min), filtered (0.22 μm), and lyophilized to obtain HD-CDs, SB-CDs, FS-CDs, and AP-CDs.

DECs were prepared by traditional boiling extraction. Herbs were soaked in a 10-fold volume of water for 30 min, and then decocted twice, with each decoction lasting for 30 min. The combined extracts were concentrated to 500 mg/mL crude drug equivalent, filtered, and freeze-dried to obtain HD-DEC, SB-DEC, FS-DEC, and AP-DEC.

CDs and DECs characterization: Morphology was characterized using TEM and HR-TEM. Functional groups were analyzed by FTIR. The surface elemental composition of CDs was determined by XPS. UV-vis absorption and fluorescence spectra were recorded to evaluate optical properties.

Cell culture and in vitro experiment: The canine mammary tumor cells (CMT-U27) were cultured in DMEM containing 10% FBS and 1% penicillin-streptomycin at 37 ℃ in a humidified incubator with 5% CO_2.

Cell viability was assessed using a CCK-8 assay. CMT-U27 cells (1×10^4/well) were seeded in 96-well plates and treated with CDs or DECs at different concentrations for 24 or 48 h. CCK-8 solution (10%) was added for 30 min, and absorbance was measured at 450 nm.

For colony formation, cells (1×10^3/well) were treated with 0.25 or 0.5 mg/mL samples for 48 h, followed by incubation in drug-free medium for 14 days. The resulting colonies were subsequently fixed, stained with crystal violet, and counted.

Cell migration was evaluated using a wound healing assay. Confluent cell monolayers were mechanically scratched and maintained in serum-free medium containing different sample concentrations (0-0.5 mg/mL). Images were taken at 0, 12, and 24 h, and wound closure was analyzed with ImageJ, from which the wound healing rate was determined using the following formula: Wound closure (%) = (1- gap area after treatment/initial gap area) ×100%.

Tumor-bearing mouse model and treatment: BALB/c nude mice (4-week-old) were subcutaneously injected with 5×10^6 CMT-U27 cells. Treatment began when tumors reached ~50 mm^3. Mice were divided into 10 groups (n=5): control, CAP (100 mg/kg), and eight CD/DEC groups (500 mg/kg). All treatments were administered by oral gavage once daily for 14 days. Tumor volume and body weight were monitored every 2 days. The whole animal experiment was conducted strictly in accordance with the relevant regulations of China Agricultural University and was approved by the Experimental Animal Welfare and Animal Experiment Ethics Review Committee of China Agricultural University. The approval number was AW32303202-2-2.

Histopathological evaluation: The tumor, heart, liver, spleen, lung and kidney were fixed in 4% paraformaldehyde solution. Terminal deoxynucleoitidyl transferase-mediated dUTP nick end labeling (TUNEL)

staining was performed in tumor tissues. Besides, the oxygens were stained with hematoxylin and eosin (H&E) for histological analysis.

Statistical analysis: Data are presented as mean ± standard deviation (SD). Statistical significance was determined using GraphPad Prism 8.0. For multiple comparisons, one-way ANOVA followed by Tukey's post-hoc test was applied. Two-group comparisons were evaluated using the unpaired t-test. $P<0.05$ was considered significant.

RESULTS

Characterization of CDs: TEM and HR-TEM revealed that all four TCM-derived CDs exhibited spherical morphology and a uniform size distribution (1-5 nm). Clear lattice fringes were observed with a consistent spacing of ~0.315 nm, corresponding to the (002) plane of graphitic carbon, indicating the presence of graphitized structures (Fig. 1).

The FTIR spectra of the CDs showed similar infrared absorption peaks, with bands near 1636 cm^{-1} and 3270 cm^{-1} attributed to the stretching vibrations of C=O, O-H and N-H bonds, respectively (Fig. 2A, D, G and J). These features indicate the presence of electron-rich groups such as carbonyl, hydroxyl and amino groups, on the CDs.

UV-vis spectra showed strong absorption in the 200-300 nm region, with a peak near 275 nm, suggesting π–π* transitions of aromatic C=C/C=N and confirming the formation of a graphitic core (Fig. 2B, E, H and K). The aqueous solution of the CDs was yellow under natural light and emitted blue or blue-green light under UV at 365 nm (inset in Fig. 2B, E, H and K). Photoluminescence (PL) spectra showed that the emission peaks of the four CDs gradually shifted with increasing excitation wavelength (Fig. 2C, F, I and L), indicating that they all exhibit excitation-dependent fluorescence, which is similar to previous studies.

To further determine the composition and structure of the four CDs, XPS was used to detect the three elements C, N and O in the CDs, and their contents were calculated from the integral area. The results show that the C content in the four CDs was the highest, and the N content was the lowest, at about 60% and 2%, respectively. Furthermore, high-resolution XPS spectra clearly showed that these four CDs have similar structures. The C1s spectra revealed peaks corresponding to C=C, C–O/C–N, and C=O bonds (Fig. 3B, F, J and N). The high-resolution XPS spectra of N1s showed two fitting bands, assigned to N-H or C-N and C=N (Fig. 3C, G, K and O). The O1s spectra showed two bands corresponding to the C=O and C-O bonds (Fig. 3D, H, L and P).

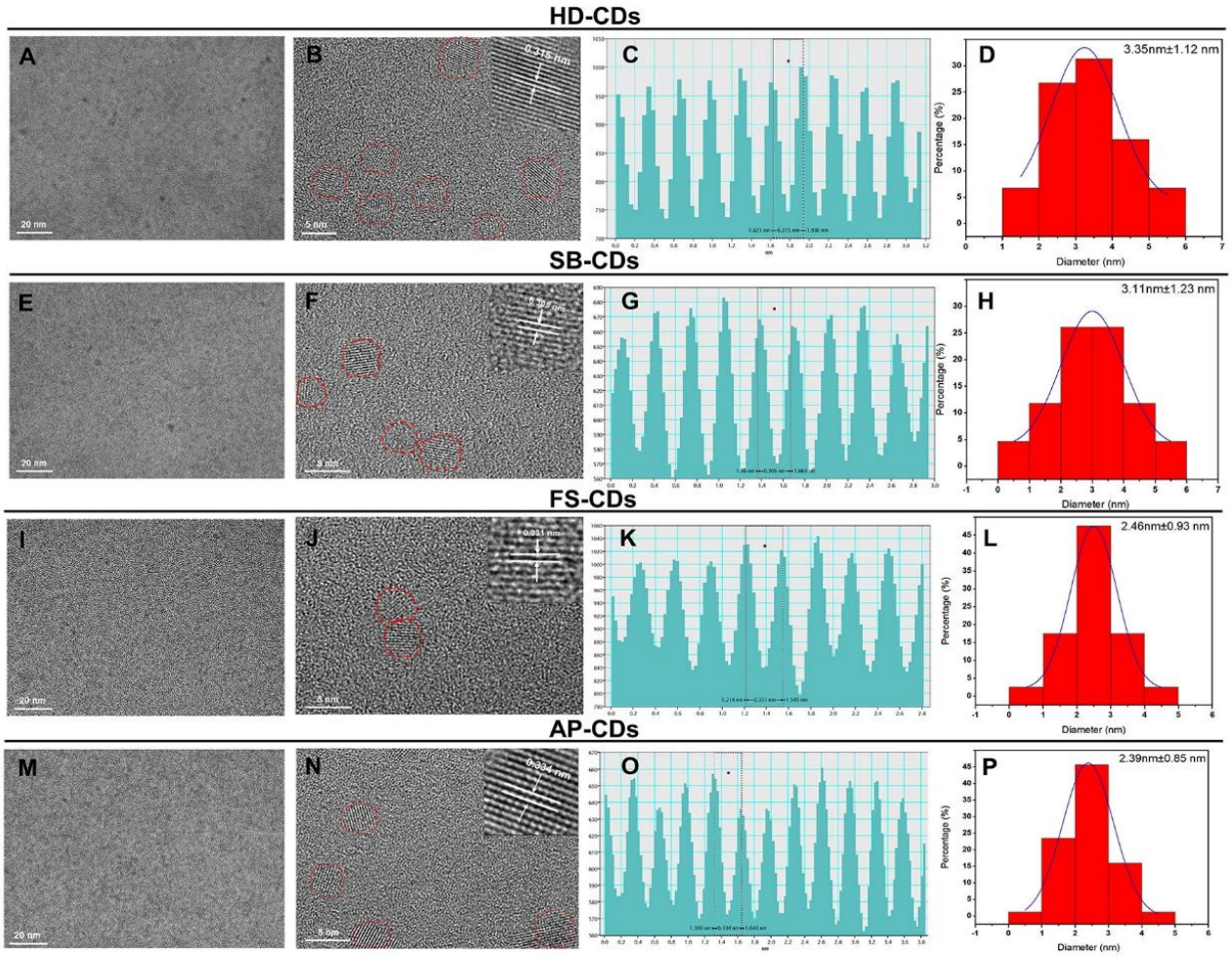

Fig. 1: Morphological characterization of four CDs. TEM images of HD-CDs (A), SB-CDs (E), FS-CDs (I) and AP-CDs (M). HR-TEM images of HD-CDs (B), SB-CDs (F), FS-CDs (J) and AP-CDs (N). Lattice spacing measurement of HD-CDs (C), SB-CDs (G), FS-CDs (K) and AP-CDs (O). Size distribution of HD-CDs (D), SB-CDs (H), FS-CDs (L) and AP-CDs (P).

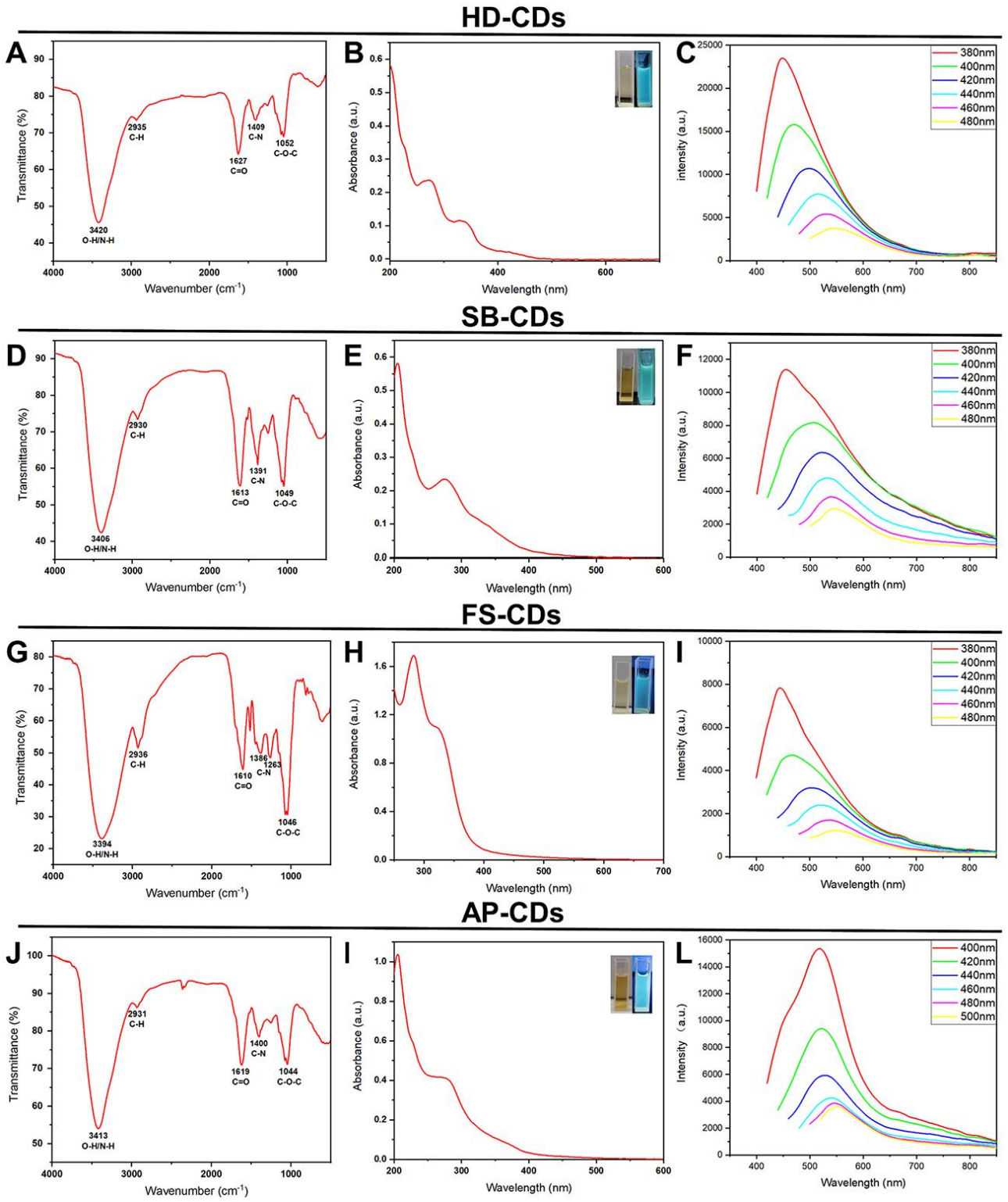

Fig. 2: Spectroscopic characterization of four CDs. FTIR spectra of HD-CDs (A), SB-CDs (D), FS-CDs (G) and AP-CDs (J). UV–vis absorption spectra of HD-CDs (B), SB-CDs (E), FS-CDs (H) and AP-CDs (K). Fluorescence emission spectra of HD-CDs (C), SB-CDs (F), FS-CDs (I) and AP-CDs (L).

The effect of four CDs on tumor cell proliferation inhibition: Both CDs and DECs could inhibit the proliferation of CMT-U27 canine mammary tumor cells (Fig. 4). However, the survival rate of CMT-U27 cells treated with CDs at different concentrations was consistently lower than that of cells treated with the corresponding DECs at the same concentrations at both 24 h and 48 h. At 48 h, the IC_{50} of all CDs was significantly lower than that of the corresponding DECs ($P<0.05$). These results indicated that CDs are more effective than DECs in inhibiting the proliferation of canine mammary tumor cells.

The effect of four CDs on tumor cell clonogenicity repression: To further compare the effects of CDs and DECs on the proliferation and clonogenic ability of single tumor cells, CMT-U27 cells were treated with CDs and DECs at 0.25 mg/mL and 0.5 mg/mL for 48 h, respectively,

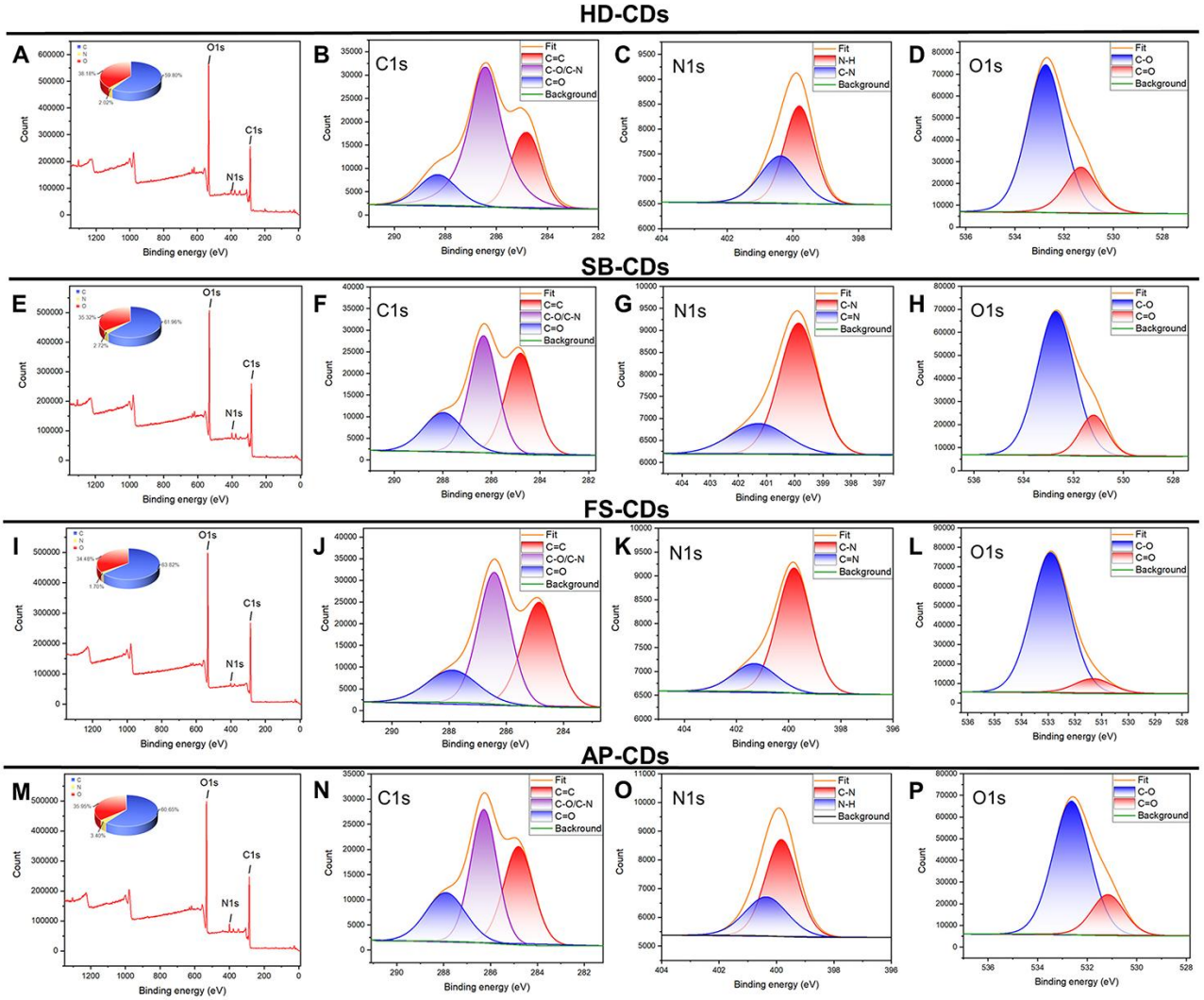

Fig. 3: The XPS spectrum of four CDs. Full XPS spectrum of HD-CDs (A), SB-CDs (E), FS-CDs (I) and AP-CDs (M). The high-resolution C1s XPS spectrum of HD-CDs (B), SB-CDs (F), FS-CDs (J) and AP-CDs (N). N1s XPS spectrum of HD-CDs (C), SB-CDs (G), FS-CDs (K) and AP-CDs (O). O1s high-resolution XPS spectra of HD-CDs (D), SB-CDs (H), FS-CDs (L) and AP-CDs (P).

and then cultured in fresh medium without drug for 14 days to assess colony formation. The results showed that CDs and DECs significantly diminished the colony formation rate of CMT-U27 cells (Fig. 5). Compared with the DECs group, the group treated with CDs showed a significant reduction in colony formation rate, which is consistent with the CCK-8 results.

The impact of four CDs on tumor cell migration inhibition: To compare the effect of CDs and DECs on the migration of mammary tumor cells, CMT-U27 cells were treated with CDs and DECs at different concentrations in serum-free medium. After 0 h, 12 h and 24 h, the migration of CMT-U27 cells was evaluated by measuring the area and width of the gap. The results showed that CDs and DECs treatment significantly inhibited cell migration during 24 h and 48 h (Fig. 6). Notably, only HD-CDs and FS-CDs exhibited superior inhibitory effects on CMT-U27 migration compared to their corresponding DECs, whereas SB-CDs and AP-CDs did not show similar advantages, revealing a subtle inconsistency with the cell proliferation study.

The antitumor ability of four CDs in vivo: To further investigate the antitumor activity of CDs in vivo, the xenograft tumor model was established using BALB/c nude mice. After 14 days of continuous oral gavage administration, the tumor growth inhibition of CDs and DECs was compared. The tumor growth curves and tumor weights indicated that CDs displayed antitumor effects in vivo, with efficacy comparable to that of the chemotherapeutic drug CAP, but not significantly different from that of DECs (Fig. 7).

The TUNEL assay was also performed to evaluate the pro-apoptotic efficacy of CDs and DECs in this study. The results showed that there were no statistically significant differences between the CDs and DECs groups in terms of TUNEL-positive cell expression levels, indicating comparable levels of apoptosis induction between the two treatments (Fig. 8). The body weight and histopathological sections of mice were further analyzed to assess the in vivo safety of CDs. It was found that no obvious abnormalities were observed in the mice from the CDs groups compared with the saline control group (Fig. 9 and 10). The results indicated that CDs have good biocompatibility and low toxicity.

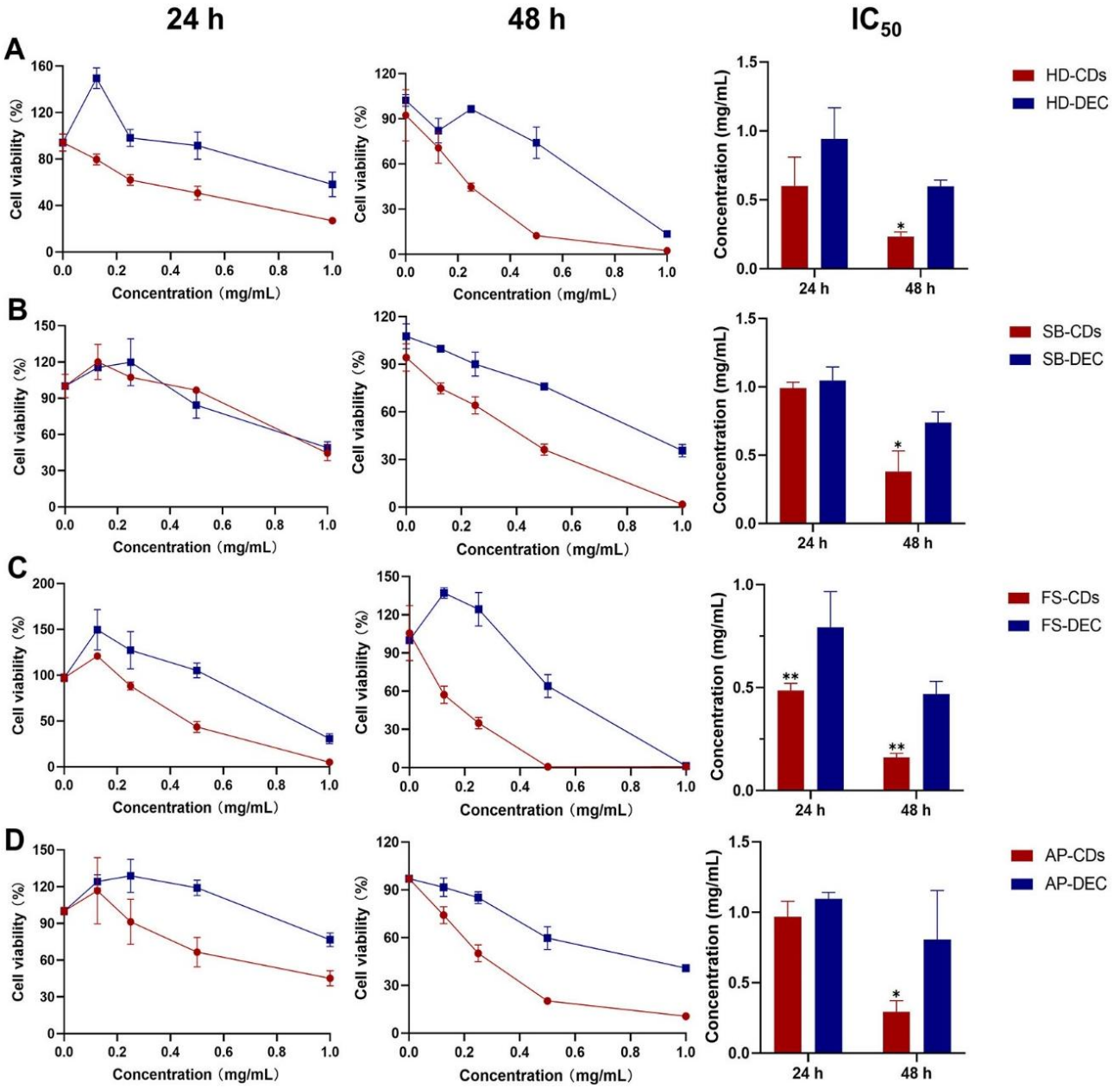

Fig. 4: Comparison of the inhibitory effect of CDs and DECs on canine mammary tumor cell CMT-U27 proliferation. CCK-8 was used to detect the cell viability of CMT-U27 after 24 h and 48 h treatment with HD-CDs and HD-DEC (A), SB-CDs and SB-DEC (B), FS-CDs and FS-DEC (C) and AP-CDs and AP-DEC (D) at different concentrations. Compared with the corresponding DEC group, **P*<0.05, ***P*<0.01.

Structure and chemical composition of DECs: The TEM images shown that individual nanoparticles cannot be clearly observed from the DECs, but instead tended to cluster together to form distinct aggregated structures (Fig. 11). Some structures even closely resembled the raw medicinal materials, such as the HD-DEC (Fig. 11A). The FTIR spectra revealed that CDs and DECs exhibited similar infrared absorption peaks (Fig. 2 and 11). This similarity indicates that the CDs might retain certain functional groups derived from the TCM precursors during the high-temperature synthesis, presenting a surface chemical profile partially consistent with that of the traditional DECs.

DISCUSSION

The results demonstrated that the four TCM-derived CDs possessed uniform nanoscale structures (1-5 nm) and analogous graphitic cores. The presence of abundant surface functional groups contributes to their excellent hydrophilicity and observed biological activities (Zhou *et al.,* 2010; Kumar *et al.,* 2012), aligning with previous findings on biomass-derived CDs (Javed and O'carroll, 2021). The structure and optical properties of the four CDs were similar, which may be largely related to the fact that their synthetic precursors are plant biomass materials and all of them were prepared by hydrothermal method, suggesting that CDs with specific microstructure can be prepared by controlling raw materials and synthesis methods.

HD, SB, FS and AP are all antitumor TCM with heat-clearing and detoxifying properties (Bao *et al.,* 2016; Lv *et al.,* 2021; Jiao *et al.,* 2026). This study found that the antitumor activity of CDs derived from these four herbs was largely associated with the activity of the corresponding raw materials. Among the DECs, FS-DEC

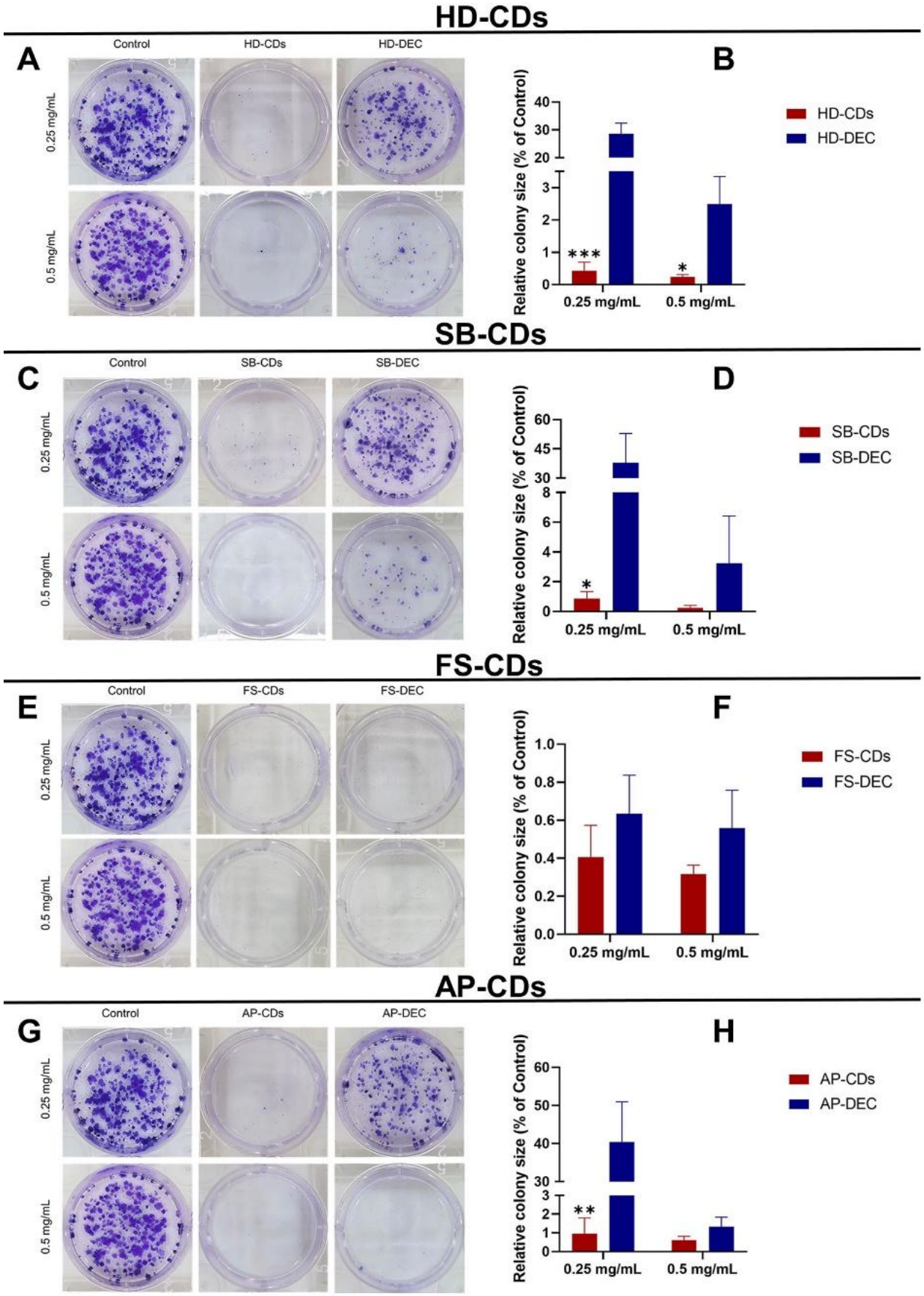

Fig. 5: Comparison of the repression effect of CDs and DECs on canine mammary tumor cell CMT-U27 clonogenic ability. Crystal violet staining of clone formation of CMT-U27 cells treated with HD-CDs and HD-DEC (A), SB-CDs and SB-DEC (C), FS-CDs and FS-DEC (E) and AP-CDs and AP-DEC (G) at different concentrations. Relative clone formation rates of CMT-U27 cells treated with HD-CDs and HD-DEC (B), SB-CDs and SB-DEC (D), FS-CDs and FS-DEC (F) and AP-CDs and AP-DEC (H) at different concentrations and the control group was used as the standard. Compared with the corresponding DEC group, *P<0.05, **P<0.01, ***P<0.001.

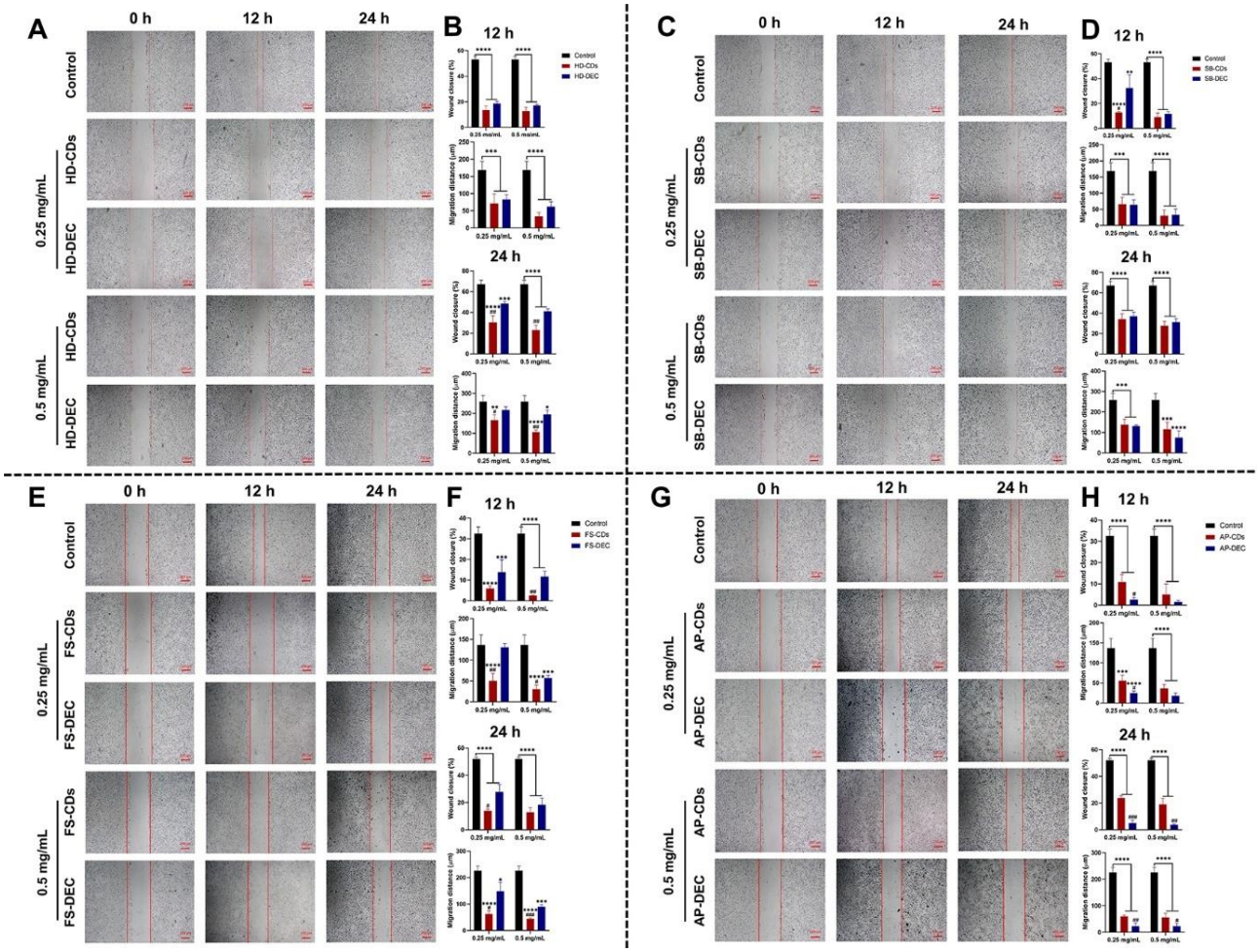

Fig. 6: Comparison of effect of CDs and DECs on inhibiting migration of canine mammary tumor cells CMT-U27. Representative pictures of CMT-U27 cells cultured with the different concentration of HD-CDs and HD-DEC (A), SB-CDs and SB-DEC (C), FS-CDs and FS-DEC (E) and AP-CDs and AP-DEC (G) after 24 h and 48 h, scale bar: 200 μm. The rate of wound closure and migration distance of boundary of CMT-U27 cultured with HD-CDs and HD-DEC (B), SB-CDs and SB-DEC (D), FS-CDs and FS-DEC (F) and AP-CDs and AP-DEC (H) at different concentrations after 12 h and 24 h. Compared with the Control group, *P<0.05, **P<0.01, ***P<0.001, ****P<0.0001; compared with the corresponding DEC group, #P<0.05, ##P<0.01, ###P<0.001.

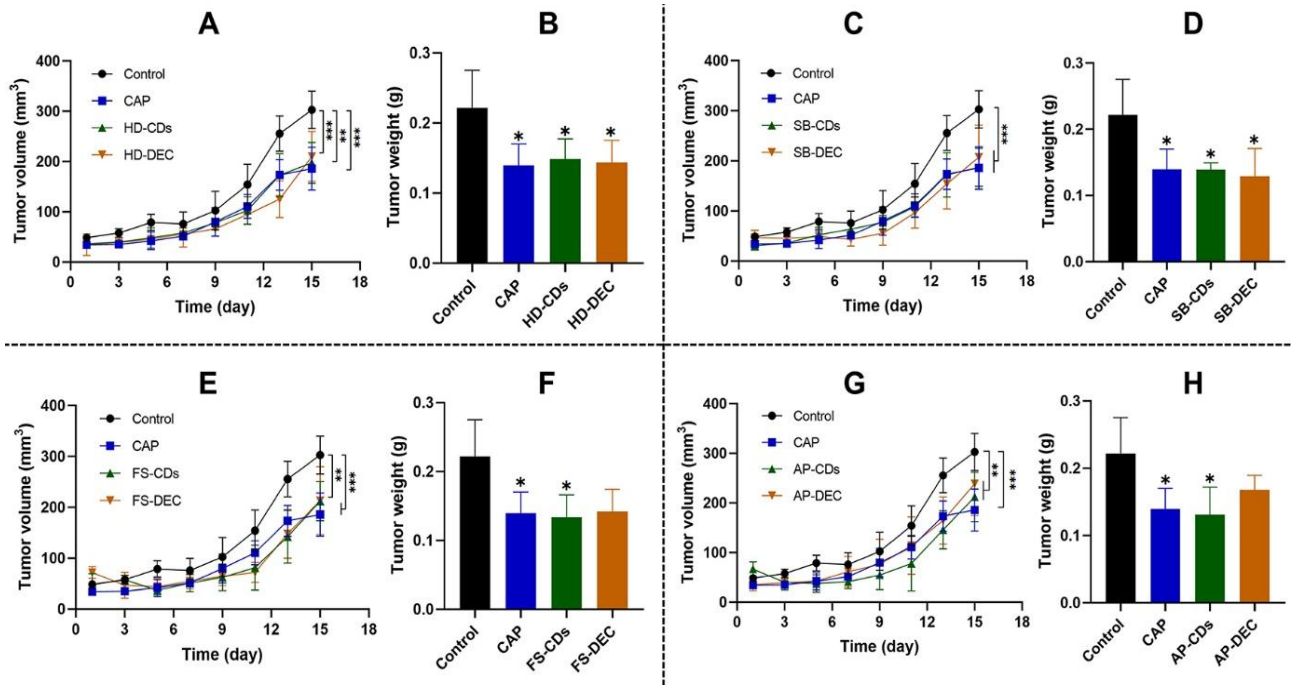

Fig. 7: Comparison of antitumor ability of CDs and DECs in vivo. Tumor growth curves of mice treated with HD-CDs and HD-DEC (A), SB-CDs and SB-DEC (C), FS-CDs and FS-DEC (E) and AP-CDs and AP-DEC (G); (C) Tumor weight of mice treated with HD-CDs and HD-DEC (B), SB-CDs and SB-DEC (D), FS-CDs and FS-DEC (F) and AP-CDs and AP-DEC (H). Compared with the Control group, *P<0.05, **P<0.01, ***P<0.001.

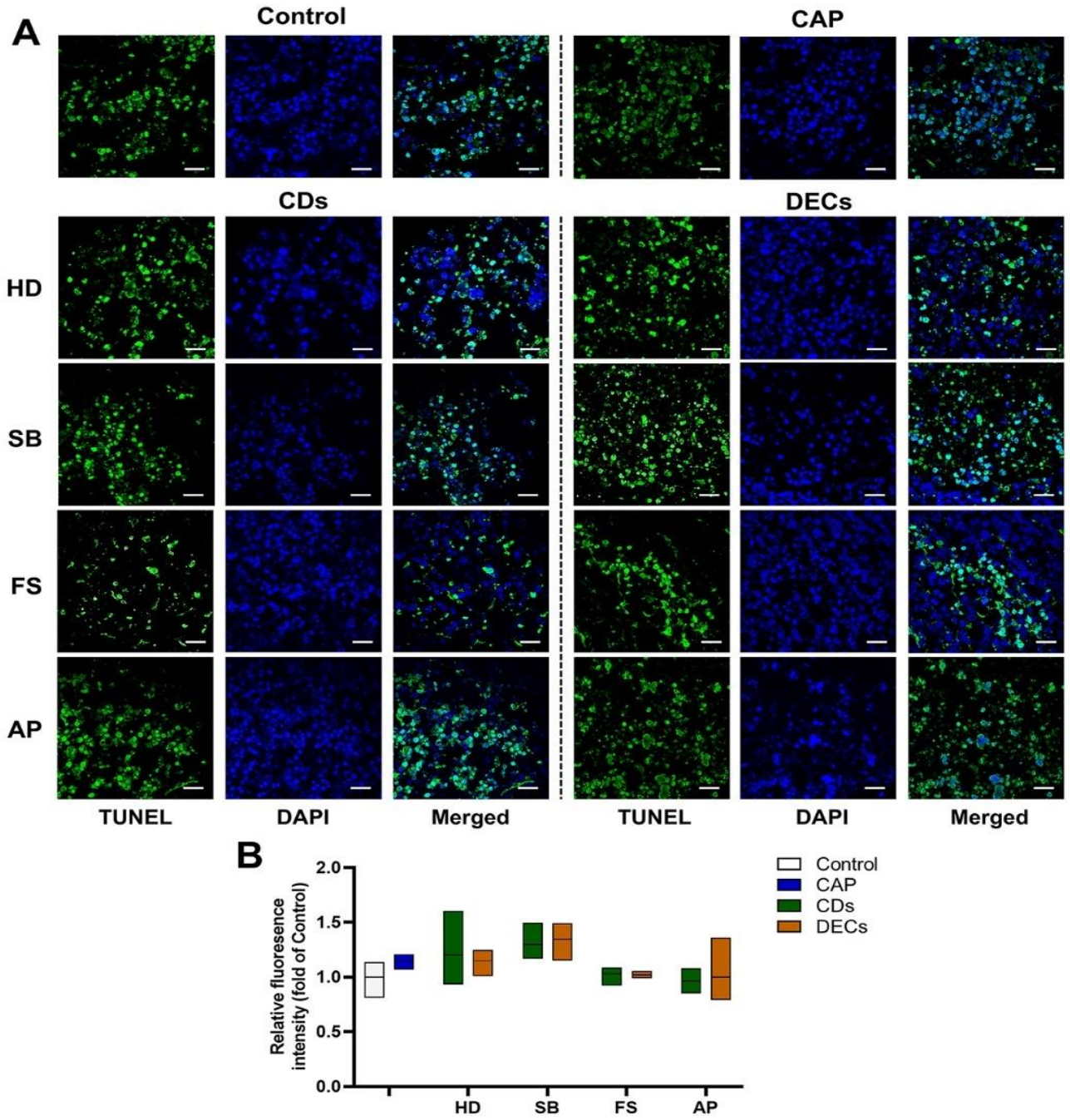

Fig. 8: TUNEL analyses of tumor sections. (A) Confocal images showing nuclei stained with DAPI in blue and TUNEL-positive nuclei stained in green. The scale bar represents 20 μm. (B) Quantification of relative fluorescence of TUNEL staining intensity (fold of Control).

exhibited the strongest inhibitory effect on CMT-U27 cell proliferation, while SB-DEC showed the weakest effect. Among the four CDs, FS-CDs showed the strongest proliferation inhibitory effect, whereas SB-CDs exhibited the weakest, which was in agreement with the results observed for the DECs. In addition, the results of cell migration assay were generally consistent with this trend, suggesting that CDs with stronger antitumor activity can be obtained by selecting precursor TCM with superior intrinsic antitumor effects. To ensure a fair comparison, both formulations were normalized by the lyophilized dry weight of the final products, allowing for a weight-for-weight evaluation of the therapeutic advantages gained from the 'nano-state' transformation. Admittedly, while serum-free conditions were used to limit proliferation, the observed scratch closure inhibition likely reflects a combined effect of reduced cell motility and inherent cytotoxicity. Furthermore, this study focused on preliminary comparative efficacy, with the absence of detailed mechanistic investigations remaining a limitation for the current biological interpretation.

The pharmacological effect of TCM is closely related to its unique chemical composition and physical state (Wu *et al.,* 2020; D'aloia *et al.,* 2022). It has been reported that particles present in DECs play an important role and act as key components that enhance the adsorption of active constituents (Nie *et al.,* 2024). The relatively large particle size enables prolonged circulation of the drug particles in vivo, which is crucial for achieving efficient tumor accumulation. However, the ultra-small size of CDs may make it easier for them to pass through cell membranes and be taken up by cells (Li *et al.,* 2023). The size of the

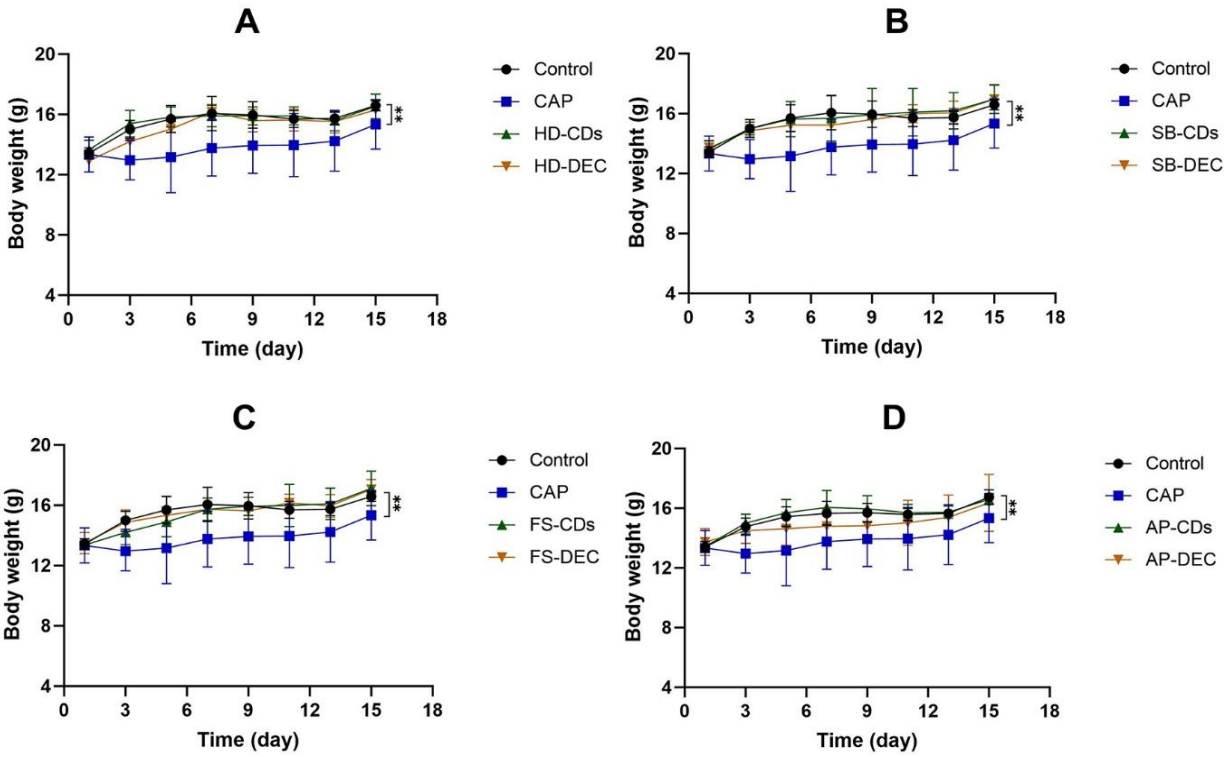

Fig. 9: Body weight of mice treated with HD-CDs and HD-DEC (A), SB-CDs and SB-DEC (B), FS-CDs and FS-DEC (C) and AP-CDs and AP-DEC (D). Compared with the Control group, **P<0.01.

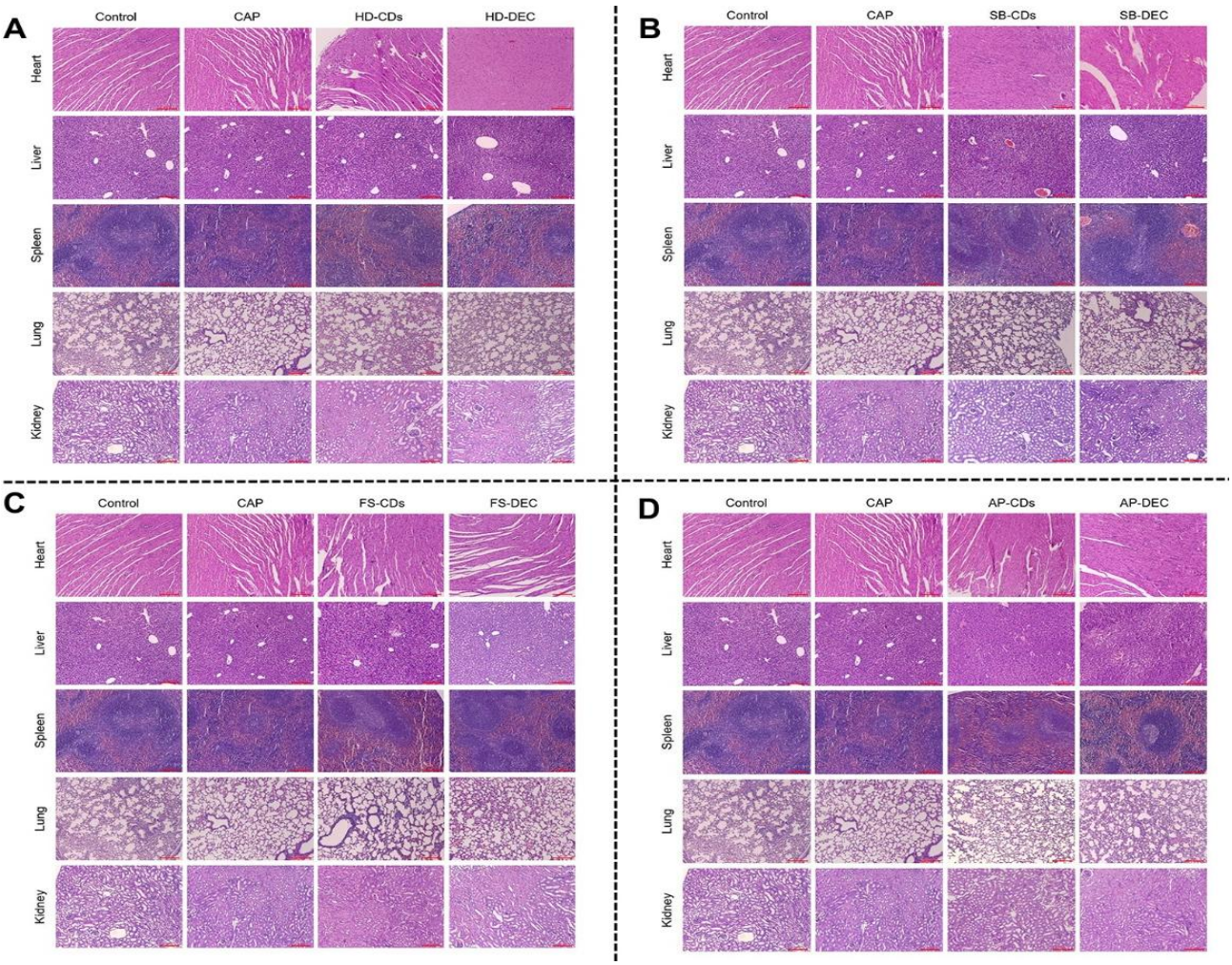

Fig. 10: Histopathological changes after HD-CDs and HD-DEC (A), SB-CDs and SB-DEC (B), FS-CDs and FS-DEC (C) and AP-CDs and AP-DEC (D) treatment. Magnification×10. The scale bar represents 200 μm.

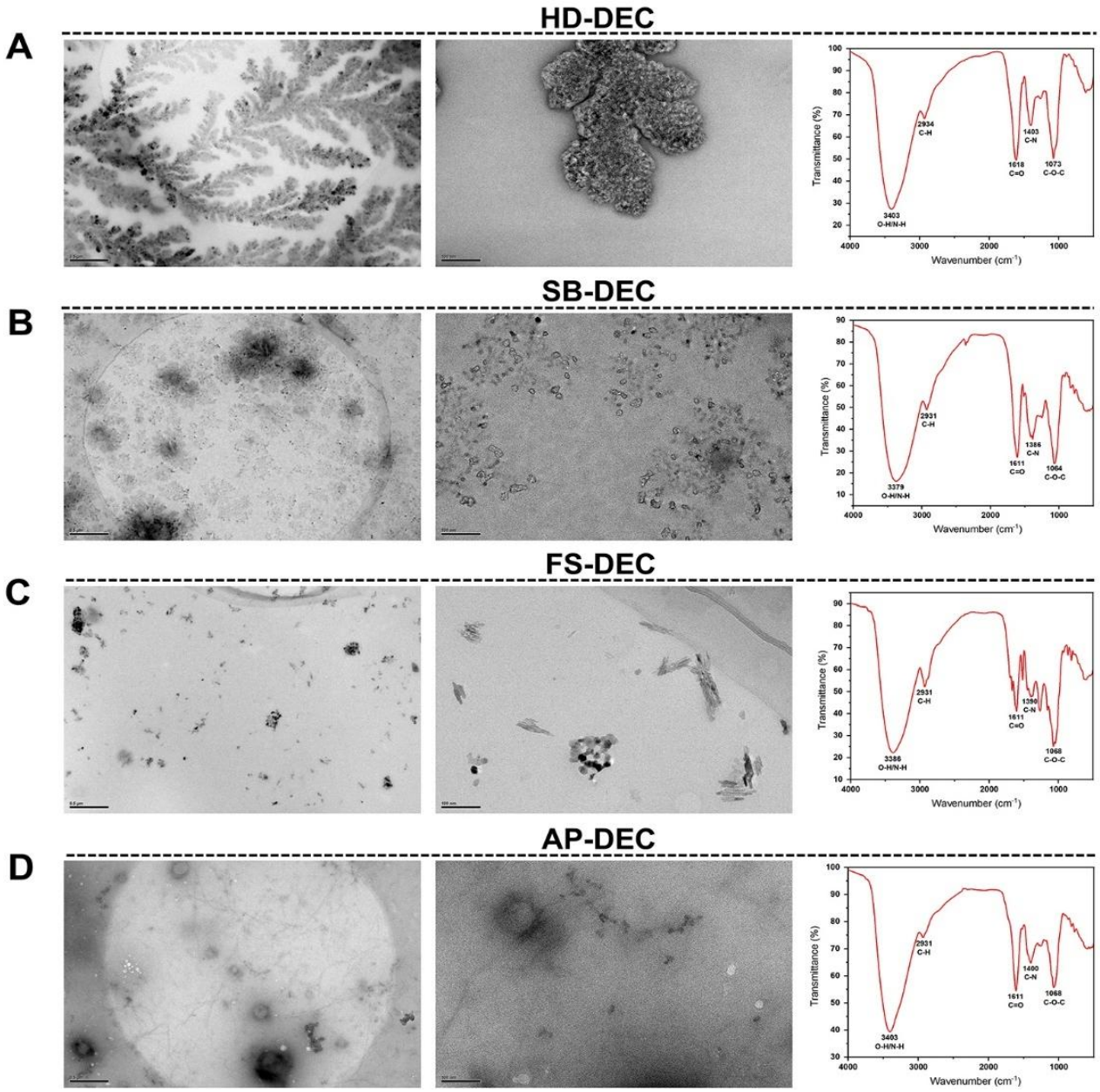

Fig. 11: Characterization of TCM DECs. TEM images and FTIR spectra of HD-DEC (A), SB-DEC (B), FS-DEC (C) and AP-DEC (D).

CDs was only around 1-5 nm (Fig. 1), which may partly explain why the CDs are more effective than the DECs in vitro, but are likely limited by distinct biophysical constraints in vivo. Specifically, although pharmacokinetic data were not directly measured, this size range sits below the established renal filtration threshold (~5.5 nm), suggesting the CDs are physically predisposed to rapid renal clearance (Choi *et al*., 2007). This provides a plausible explanation for the current in vivo results, as rapid excretion may limit sustained accumulation at the target site. Beyond these biophysical constraints, the structural clarity of the therapeutic agent is equally vital. While DECs are the complex systems comprising small molecules, particle aggregates, and precipitates, and their exact composition remains unclear (Nie *et al.,* 2024), CDs possess a more defined and consistent chemical structure. This structural advantage may simplify the standardization and optimization of TCM-derived therapeutics. Nevertheless, as an exploratory investigation, this study utilized a sample size (n=5) aligned with the 3Rs principle for preliminary screening, which may have limited the statistical power to detect subtle differences between the treatment groups.

Addressing the rapid renal clearance of ultra-small CDs while maintaining their deep tissue penetration remains a critical challenge, which may be potentially resolved by integrating them into multistage cooperative nanoplatforms. Hou et al. designed a transformable honeycomb-like nanoassemblies based on CDs that prevented rapid renal clearance to extend circulation, while disassembling into small CDs for deep tumor penetration and maximized therapeutic efficacy (Hou *et al*., 2021). FTIR and XPS results revealed that CDs possess abundant surface functional groups, such as hydroxyl and amino groups, which could serve as reactive sites for such functional modifications to potentially enhance their in vivo antitumor efficacy in future studies. In addition, while DECs are traditionally limited to oral

administration, the small size and good biocompatibility of CDs provide the technical possibility for systemic administration, which warrants further investigation to determine if it can improve bioavailability and therapeutic outcomes compared to traditional forms.

Conclusions: In this work, four types of CDs (HD-CDs, SB-CDs, FS-CDs and AP-CDs) were synthesized by a one-step hydrothermal method using Chinese herbs HD, SB, FS and AP as carbon sources. In vitro, these four CDs effectively inhibited the proliferation and migration of canine mammary tumor cells CMT-U27, and their effects were generally superior to those of the corresponding DECs. The in vivo results showed that the four CDs effectively inhibited the growth of CMT-U27. Although their antitumor effects were not significantly different from those of DECs, they may still possess potential advantages.

Acknowledgment: This work was financially supported by the National Nature Science Foundation of China (Grant no. 32373056, Grant no. 82100819), the 14th Five-Year Plan National Key Research and Development Program of China (2022YFD1801104), the 2115 Talent Development Program of China Agricultural University (Grant no. 00109023), the Large Research Project of the Deanship of Research and Graduate Studies at King Khalid University (R.G.P.2/243/47) and the Princess Nourah bint Abdulrahman University Researchers Supporting Project (PNURSP2026R224).

Author contributions: Qi Chen: Experimental conduction, Writing, Visualization. Biao Liu: Experimental conduction, Visualization. Zixiang Lin: Experimental conduction. Xinqiu Li: Visualization, Experimental conduction. Fangying Zhao: Experimental conduction. Chengyu Liu: Experimental conduction. Hong Zhang: Visualization. Wanbing Pan: Experimental conduction. Jiatong Zhang and Delanyo Kpeglo: Writing-review. Ramadan Taha, Maha Abdullah Momenah and Etibar Mammadov: Funding acquisition. Wen Chen: Conceptualization, Data curation, Writing-review, Funding acquisition. Jiahao Lin: Conceptualization, Data curation, Writing-review, Funding acquisition. All authors have read and agreed to the published version of the manuscript.

REFERENCES

Bao J, Ding R, Zou L, *et al.,* 2016. Forsythiae fructus inhibits B16 melanoma growth involving MAPKs/Nrf2/HO-1 mediated anti-oxidation and anti-inflammation. The American journal of Chinese medicine 44:1043-1061.

Beaudu-Lange C and Lange E, 2024. Intensive Multimodal Chemotherapy in a Dog Suffering from Grade III/Stage IV Solid Mammary Carcinoma. Animals 14:2618.

Choi HS, Liu W, Misra P, *et al*., 2007. Renal clearance of nanoparticles. Nature biotechnology 25:1165.

Cohen EN, Kondiah PP, Choonara YE, *et al.*, 2020. Carbon dots as nanotherapeutics for biomedical application. Current pharmaceutical design 26:2207-2221.

D'aloia A, Ceriani M, Tisi R, Stucchi S, *et al.*, 2022. Cannabidiol antiproliferative effect in triple-negative breast cancer MDA-MB-231 cells is modulated by its physical state and by IGF-1. International journal of molecular sciences 23:7145.

Fang M, Wang B, Qu X, Li S, *et al.,* 2024. State-of-the-art of biomass-derived carbon dots: Preparation, properties, and applications. Chinese Chemical Letters 35:108423.

Ferreira T, Dias F, Gama A, *et al*., 2026. Hallmarks of cancer in canine mammary tumors: Insights into a potential model for human triple-negative breast cancer. Critical Reviews in Oncology/Hematology 105184.

Hou L, Chen D, Wang R, *et al.,* 2021. Transformable honeycomb-like nanoassemblies of carbon dots for regulated multisite delivery and enhanced antitumor chemoimmunotherapy. Angewandte Chemie 133:6655-6666.

Huang C, Dong M, Luo J, *et al.,* 2020. The activity screening of Hmong herbs Caesalpiniaminax and an antitumor effect study. Evidence-Based Complementary and Alternative Medicine 2020:3585736.

Javed N and DM O'carroll, 2021. Carbon dots and stability of their optical properties. Particle & Particle Systems Characterization 38:2000271.

Jiao C, Zhang T, Yang Y, *et al.,* 2026. Progress in Research on Alleviating the Symptoms Associated With Advanced Cancer Using Traditional Chinese Medicine. Pain Research and Management 2026:7197339.

Kumar D, Kumar M, Saravanan C, *et al.,* 2012. Curcumin: a potential candidate for matrix metalloproteinase inhibitors. Expert opinion on therapeutic targets 16:959-972.

Li CL, Ou CM, Huang CC, *et al.,* 2014. Carbon dots prepared from ginger exhibiting efficient inhibition of human hepatocellular carcinoma cells. Journal of Materials Chemistry B 2:4564-4571.

Li J, Fu W, Zhang X, *et al.,* 2023. Green preparation of ginger-derived carbon dots accelerates wound healing. Carbon 208:208-215.

Liu L, Liu T, Tao W, *et al.,* 2022. Flavonoids from Scutellaria barbata D. Don exert antitumor activity in colorectal cancer through inhibited autophagy and promoted apoptosis via ATF4/sestrin2 pathway. Phytomedicine 99:154007.

Luo WK, Zhang LL, Yang ZY, *et al.,* 2021. Herbal medicine derived carbon dots: synthesis and applications in therapeutics, bioimaging and sensing. Journal of Nanobiotechnology 19:320.

Lv YX, Pan HR, Song XY, *et al.,* 2021. Hedyotis diffusa plus Scutellaria barbata Suppress the Growth of Non-Small-Cell Lung Cancer via NLRP3/NF-κB/MAPK Signaling Pathways. Evidence-Based Complementary and Alternative Medicine 2021:6666499.

Ma C, Wei Y, Liu Q, *et al.,* 2019. Polysaccharides from Hedyotis diffusa enhance the antitumor activities of cytokine-induced killer cells. Biomedicine & Pharmacotherapy 117:109167.

Nie W, Liu Y, Lan J, *et al.,* 2024. Self-assembled nanoparticles from xie-bai-san decoction: isolation, characterization and enhancing oral bioavailability. International Journal of Nanomedicine 3405-3421.

Seo G, Kim BS, Lim H, *et al.,* 2026. Biomedical applications and future perspectives of carbon dots and their hybrid nanomaterials. Materials Advances 7:157-174.

Tian Y, Yao J, Gao Q, *et al.,* 2025. Holistic concept guided quality control of traditional Chinese medicines for optimizing bioavailability. Chinese Medicine 20:202.

Vu TD, Nguyen TH, Nguyen VLT, *et al.,* 2026. Epidemiology, histopathological classification, hematological alterations, and treatment outcomes of canine mammary tumors in Ho Chi Minh City, Vietnam. World's Veterinary Journal 16:211-219.

Wu SH, Li HB, Li GL, *et al.,* 2020. Metabolite identification of gut microflora-cassia seed interactions using UPLC-QTOF/MS. Experimental and Therapeutic Medicine 19:3305-3315.

Wu Y, Huang J, Guo J, *et al.,* 2025. Drug repurposing in traditional Chinese medicine: from empirical wisdom to modern therapeutic strategies. Frontiers in Pharmacology 16:1631727.

Xie Y, Liu H, Teng Z, *et al.,* 2025. Nanomaterial-enabled anti-biofilm strategies: new opportunities for treatment of bacterial infections. Nanoscale 17:5605-5628.

Yan G, Wang Y, Han X, *et al.,* 2019. A modern technology applied in traditional Chinese medicine: Progress and future of the nanotechnology in TCM. Dose-Response 17:1559325819872854.

Yao H, Li J, Song Y, *et al.,* 2018. Synthesis of ginsenoside Re-based carbon dots applied for bioimaging and effective inhibition of cancer cells. International journal of nanomedicine 6249-6264.

Yu L and Gai Y, 2023. Elucidating the mechanism of agrimonolide in treating colon cancer based on network pharmacology. Drug Design, Development and Therapy 2209-2222.

Yu W, Chen M, Tan X, *et al.,* 2026. Traditional chinese medicine modernization in diagnosis and treatment: Utilizing artificial intelligence and nanotechnology. MedComm 7:e70596.

Zhou T, Shi Q, Chen CH, *et al.,* 2010. Anti-AIDS agents 79. Design, synthesis, molecular modeling and structure–activity relationships of novel dicamphanoyl-2′, 2′-dimethyldihydropyranochromone (DCP) analogs as potent anti-HIV agents. Bioorganic & Medicinal Chemistry 18:6678-6689.